Metal-insulator transition in one-dimensional quasi-periodic systems

1991 J. Phys.: Condens. Matter 3 6041

(http://iopscience.iop.org/0953-8984/3/32/011)

J. Phys.: Condens. Matter 3 (1991) 6041–6053. Printed in the UK

Metal–insulator transition in one-dimensional quasi-periodic systems

Chaitali Basu†, Abhijit Mookerjee†, Asok K Sen‡ and Prabhat K Thakur‡

† S N Bose National Centre for Basic Sciences, DB 17, Sector 1, Salt Lake City, Calcutta 700064, India

‡ Saha Institute of Nuclear Physics, AF1, Sector 1, Bidhannagar, Calcutta 700 064, India

Received 8 January 1991

Abstract. We use the vector recursion method of Haydock to obtain the transmittance of a class of generalized Harper model in one dimension and to study the metal–insulator transition in this model. We also study the Argand map of the complex transmission coefficient which contains information about the phase change of the wavefunctions as they travel through the chain. This method of location of the metal–insulator transition is computationally easy and fast and does not require cumbersome formulae for calculating the localization length involving diagonalization of very large matrices, and assumptions of exponential localization. Moreover, we may use our methodology to analyse situations where we have non-exponential localization.

1. Introduction

Recently there has been considerable effort in understanding the nature of electronic states in quasi-periodic systems. Practical applications of such studies involve, among other things, incommensurate superlattices (Merlin *et al* 1985) and one-dimensional quasi-crystals (Kohmoto *et al* 1983, Kohmoto and Banavar 1986). While it is well known that in a one-dimensional system with random potentials *all* states are localized (Ishii 1973), and whereas *all* states are extended Bloch states in the absence of disorder, it has recently been shown (Avron and Simon 1982, Sokoloff 1984, Tang and Kohmoto 1986, Griniasty and Fishman 1988, Das Sarma *et al* 1990, Thakur *et al* 1990) that certain quasi-periodic systems in one dimension are capable of showing a transition from localized to extended states. In addition, there is interesting behaviour in the intermediate critical states.

In our present paper, we shall focus on the simple nearest-neighbour tight-binding Anderson model with a Hamiltonian of the form

$$H = \sum_n \varepsilon_n \varphi_n^\dagger \varphi_n + \sum_n V_{n+1}(\varphi_{n+1}^\dagger \varphi_n + \varphi_n^\dagger \varphi_{n+1}) \tag{1}$$

where $\{\varphi_n\}$ is the set of annihilation operators for the tight-binding basis orbitals. A simple quasi-crystalline model is the so-called Harper model where $\varepsilon_n = \lambda \cos(2\pi Qn + \delta)$ (Andre and Aubry 1980, Simon 1982, Sokoloff 1985). Typically the hopping energy V_n is a non-random quantity (equal to V), set equal to unity to fix the

0953-8984/91/326041 + 13 $03.50

energy scale. In this case the period Q^{-1} of the potential is incommensurate with the period of the lattice (which equals unity). When Q is irrational, the spectrum is absolutely continuous (i.e. all states are extended) for $0 < \lambda < 2$. It is point like (i.e. all states are localized) if $\lambda > 2$. In fact, an interesting duality property (Aubry duality) exists between the cases $\lambda < 2$ and $\lambda > 2$, with the case $\lambda = 2$ being self-dual. For this last case ($\lambda = 2$), all states are critical and the spectrum is singularly continuous. This self-dual case leads to a global scaling properties of the spectrum with a range of scaling indices and an associated multifractal character (Tang and Kohmoto 1986). These workers have also shown that, if Q is a rational approximant of an irrational number, e.g. $Q = F_{l-1}/F_l$, where F_l is the lth Fibonacci number, then the spectrum consists of F_l bands and F_{l-1} gaps.

The simple Aubry model in one dimension does not have a mobility edge, whereas an extension due to Griniasty and Fishman (1988) seems to have an extended localized transition at an appropriate mobility edge under certain circumstances. For this model, which is sometimes called the generalized Harper model, $\varepsilon_n = \lambda \cos(2\pi n^\gamma Q + \delta)$ and $\gamma \neq 1$. For $\gamma \geq 2$, it has been stated that the problem is equivalent to the corresponding random problem (Anderson 1958) and all states are exponentially localized. It may be noted that $\gamma \neq 1$ gives rise to an inhomogeneity in the period of the potential. It is known that inhomogeneity in the amplitude variation of the potential gives rise to a localization–delocalization transition (Souillard 1987). It will be interesting to study whether such an effect arises out of inhomogeneity of the period of the potential. The idea of inhomogeneity of the period may be easily noted if we write the potential as $\lambda \cos[2\pi n(Qn^{\gamma-1})]$. The effective period $Q' = Qn^{\gamma-1}$ is n dependent and so inhomogeneous.

Griniasty and Fishman (1988) studied the band centre states for $0 < \gamma < 1$ with Q irrational within the perturbation theory and concluded that all states are extended. In contrast, Das Sarma *et al* (1990) observed, using a heuristic argument and exact numerical calculations of eigenvalues and wave amplitudes in finite systems, that, for $0 < \gamma < 1$, $\lambda < 2$, there are mobility edges at $E_c = \pm(2V - \lambda)$, with extended states at the centre of the band $|E| < 2V - \lambda$ and localized states at the band edges $2V - \lambda < |E| < 2V + \lambda$. Further, for $1 < \gamma < 2$, they find, together with Thouless (1988), that all states away from the exact band centre are localized and the Lyapunov exponent (inverse localization length) approaches zero extremely slowly at the band centre.

Our aim is to study wave propagation in such models by numerically calculating the transmittance as a function of the energy of the incident wave and by monitoring the way in which the phase of the transmission coefficient (which is related to the phase of the electronic wavefunction) changes as the wave propagates through the medium. This will be done for all values of γ including negative values not explicitly reported so far. Our approach based on the vector recursion technique of Godin and Haydock (1988) is complementary to that of Das Sarma *et al*. The vector recursion method, as we shall indicate, is easily extended to more than one dimension, a work which we shall report in a subsequent publication. Our results are, to a large extent, in agreement with those of Das Sarma *et al*, justifying their criticism of the earlier work of Griniasty and Fishman.

2. Formalism

We shall describe a narrow wire by an Anderson tight-binding Hamiltonian of the type described in (1). The chain will be of length $2N$:

$$H_{\text{sample}} = \sum_{n=1}^{2N} [\varepsilon_n \varphi_n^\dagger \varphi_n + V(\varphi_{n+1}^\dagger \varphi_n + \varphi_n^\dagger \varphi_{n+1})]. \tag{2}$$

The V values are non-random and the energy is scaled so that $V = 1$. The diagonal terms $\varepsilon_n = \lambda \cos(2\pi n^\gamma Q)$, where Q is the irrational 'golden mean', $(\sqrt{5} - 1)/2$. If $\gamma = 1$ we have the usual Aubry model, while for $\gamma \neq 1$ we have the Griniasty–Fishman generalisation of the Aubry model. For $\gamma \neq 0$ the potential is incommensurate with the lattice.

To the two ends $n = 1$ and $n = 2N$ we attach elementary, perfectly conducting semi-infinite leads. The purpose of these leads is to bear the incoming, reflected and transmitted waves:

$$H_{\text{in}} = \sum_{n=0}^{-\infty} [\varepsilon' \varphi_n^\dagger \varphi_n + V'(\varphi_{n+1}^\dagger \varphi_n + \varphi_n^\dagger \varphi_{n+1})]$$
$$H_{\text{out}} = \sum_{n=2N+1}^{\infty} [\varepsilon'' \varphi_n^\dagger \varphi_n + V''(\varphi_{n+1}^\dagger \varphi_n + \varphi_n^\dagger \varphi_{n+1})]. \tag{3}$$

For simplicity we shall take $\varepsilon' = \varepsilon'' = 0$ and $V' = V'' = V_{\text{lead}}$.

The solution of the Schrödinger equation in the two leads are known. These are travelling Bloch waves of the form

$$\Psi_{\text{leads}} = \sum_n \psi_n \varphi_n^\dagger \tag{4}$$

with $\psi_n = A \exp(\pm in\theta)$. As the wave travels through the leads, its phase changes by θ from one site to the next. In the elementary perfectly conducting leads, this phase change is determinate:

$$\cos\theta = (E/2V_{\text{lead}}) \tag{5}$$

where E is the energy associated with the incoming wave.

We have assumed that transport is ideal in the leads right up to the contacts with the sample. This ignores boundary effects. However, if we consider large enough samples, such boundary effects are expected to be negligible.

As we shall see later, the density of states is non-zero in the region $-(2V + \lambda) \leqslant E \leqslant 2V + \lambda$. If we wish to examine the transmittance within this band, we must choose a V_{lead} which allows this full band pass, i.e. $V_{\text{lead}} \geqslant V + \lambda/2$. This is because, in order to have propagating states in the leads, we must have a real solution to equation (5).

The *vector recursion technique* (Godin and Haydock 1988) now changes to a new *vector basis* with vector annihilation operators

$$\Phi_n = \begin{pmatrix} \varphi_n \\ \varphi_{2N+1-n} \end{pmatrix}. \tag{6a}$$

In this basis, the lead and sample Hamiltonians become

$$H_{\text{sample}} = \sum_{n=1}^{N} (\mathbf{A}_n \Phi_n^\dagger \Phi_n + \mathbf{B}_{n+1} \Phi_{n+1}^\dagger \Phi_n + \mathbf{B}_{n+1}^\dagger \Phi_n^\dagger \Phi_{n+1}) \tag{6b}$$

$$H_{\text{leads}} = \sum_{n=0}^{-\infty} (\mathbf{B}_{n+1} \Phi_{n+1}^\dagger \Phi_n + \mathbf{B}_{n+1}^\dagger \Phi_n^\dagger \Phi_{n+1}) \tag{6c}$$

with

$$\mathbf{A}_n = \begin{pmatrix} \varepsilon_n & 0 \\ 0 & \varepsilon_{2N+1-n} \end{pmatrix} \qquad \text{for } 1 \leqslant n < N$$
$$\mathbf{A}_N = \begin{pmatrix} \varepsilon_N & V \\ V & \varepsilon_{N+1} \end{pmatrix} \qquad \mathbf{B}_n = \begin{pmatrix} 0 & V \\ V & 0 \end{pmatrix}. \tag{6d}$$

The Schrödinger equation may be expressed as a three-term linear difference equation involving the 2×2 matrices in (6*d*) and the wavefunction vector amplitudes

$$\Psi_n = \begin{pmatrix} \psi_n \\ \psi_{2N+1-n} \end{pmatrix}$$

$$\mathbf{B}_{n+1}^{\dagger}\Psi_{n+1} = (E\mathbf{I} - \mathbf{A}_n)\Psi_n - \mathbf{B}_n\Psi_{n-1}. \tag{7}$$

Let us now think of a situation where an incoming wave $\Sigma_n \exp(in\theta)\ \varphi_n^{\dagger}$ is travelling to the right along the input lead. As it reaches the sample, it is scattered. A reflected wave $\Sigma_n r(E) \exp(-in\theta)\ \varphi_n^{\dagger}$ travels back in the input lead to the left and a transmitted wave $\Sigma_n t(E) \exp(in\theta)\ \varphi_n^{\dagger}$ travels in the output lead. $r(E)$ and $t(E)$ are the complex reflection and transmission coefficients. Since the solutions in the leads are known, the boundary conditions in the new vector basis are

$$\Psi_0 = \begin{pmatrix} 1 + r \\ t \end{pmatrix} \qquad \Psi_1 = \begin{pmatrix} \exp(\mathrm{i}\theta) + r\exp(-\mathrm{i}\theta) \\ t\exp(-\mathrm{i}\theta) \end{pmatrix}. \tag{8}$$

Note here that we have chosen to measure our phases from the basis labelled 0 just outside the joint between the leads and the sample. It is also clear that, in the way in which we have numbered the new basis, the reflected and transmitted waves both travel to the left—hence the negative sign in the exponent of the transmitted wave.

The general solution of (7) satisfying these boundary conditions may be written in terms of the two independent family of solutions of (7) $\{\mathbf{X}_n\}$ and $\{\mathbf{Y}_n\}$, which satisfy

$$\begin{aligned} \mathbf{B}_{n+1}^{\dagger}\mathbf{X}_{n+1} &= (E\mathbf{I} - \mathbf{A}_n)\mathbf{X}_n - \mathbf{B}_n\mathbf{X}_{n-1} \qquad & \mathbf{X}_0 = \mathbf{I} \quad \mathbf{X}_1 = \mathbf{0} \\ \mathbf{B}_{n+1}^{\dagger}\mathbf{Y}_{n+1} &= (E\mathbf{I} - \mathbf{A}_n)\mathbf{Y}_n - \mathbf{B}_n\mathbf{Y}_{n-1} \qquad & \mathbf{Y}_0 = \mathbf{0} \quad \mathbf{Y}_1 = \mathbf{I}. \end{aligned} \tag{9}$$

This solution is

$$\xi_n = \mathbf{X}_n\Psi_0 + \mathbf{Y}_n\Psi_1. \tag{10}$$

Direct substitution in (7) and (8) shows that this is indeed the required solution with the correct boundary conditions.

In an exactly similar manner we can discuss the case in which the incoming wave travels to the right in the lead labelled 2. After scattering by the sample the reflected wave travels to the left in lead 2 and the transmitted wave to the left in lead 1. Here $r'(E)$ and $t'(E)$ are the reflection and transmission coefficients of this new problem, with boundary conditions

$$\Psi_0' = \begin{pmatrix} t' \\ 1 + r' \end{pmatrix} \qquad \Psi_1' = \begin{pmatrix} t'\exp(-\mathrm{i}\theta) \\ \exp(\mathrm{i}\theta) + r'\exp(-\mathrm{i}\theta) \end{pmatrix} \tag{8'}$$

and

$$\xi_n' = \mathbf{X}_n\Psi_0' + \mathbf{Y}_n\Psi_1'. \tag{10'}$$

We have a further boundary condition. Since the length of the chain is finite, in the new basis the vector chain terminates after N steps, so that

$$\xi_{N+1} = \mathbf{0} \qquad \xi'_{N+1} = \mathbf{0}. \tag{11}$$

If we substitute this in (8), (8′), (10) and (10′) we immediately obtain an expression for the scattering **S**-matrix:

$$\mathbf{S} = \begin{pmatrix} r & t \\ t' & r' \end{pmatrix} = -[\mathbf{X}_{N+1} + \mathbf{Y}_{N+1}\exp(-\mathrm{i}\theta)]^{-1}[\mathbf{X}_{N+1} + \mathbf{Y}_{N+1}\exp(\mathrm{i}\theta)]. \tag{12}$$

In the absence of magnetic fields the time-reversal symmetry gives $t = t'$. The **S**-matrix

is symmetric. Finally, the transmittance $T(E) = |t(E)|^2$ while the reflectance $R(E) = |r(E)|^2$.

It may be mentioned here that for large system sizes (greater than 10^3) we have used an ordinary recursion technique with single-site transfer matrices (see, e.g. Liu and Chao 1986) as opposed to the vector recursion technique described above. The simpler method has the advantage of being exponentially faster (in these quasi-periodic models or models with varying periods, but not in purely random impurity models) when one keeps on adding length elements to the original chain but has the disadvantage of being limited to one dimension only.

3. Results and discussion

The results reported below, except those on Argand maps of the complex transmission coefficient, are to a large extent complementary to those of Das Sarma *et al*. The recursion method has the great virtue of giving a measurable quantity (namely the transmittance) and the mobility edges can be located relatively easily with smaller size systems by looking at the transmittance rather than by first exactly diagonalizing the Hamiltonian for a much larger system and then by calculating the Lyapunov exponent (or inverse localization length) from the eigenenergies or the eigenfunctions. As an added advantage, since the transmission coefficients contain information on the wavefunction at a particular energy, one can monitor the change in the electronic phase at successive scatterings. Further, since by using the transfer matrix method and applying the Landauer formula one can calculate the conductance directly as a function of length, one can check the validity of the one-parameter scaling theory. One may also study the form of the renormalization group flow within this one-parameter scaling and locate its fixed point (or points, if there is more than one). This we shall discuss in a subsequent paper. For all the results presented below, the non-random hopping term has been set at $V = 1$. Most of our calculations are done on chains of length 10^5.

Figure 1(*a*) shows the transmittance versus energy of the incoming wave for the pure Aubry model ($\gamma = 1.0$) with $\lambda = 1$. The transmittance fluctuations characteristic of incommensurate systems are clearly visible. These, in turn, lead to strong fluctuations in conductance with changes in the chemical potential (Thakur *et al* 1990). In figure 1(*b*), we show the density of states (DOS) for the same situation. The DOS strongly resembles that of a model where the site-diagonal terms are in a Fibonacci sequence. In the Aubry model, the site-diagonal terms are incommensurate with the underlying lattice. However, the qualitative feature of the DOS (e.g. the gap structures) do not seem to be very different in these two cases. These two figures together show that *all* states are extended in this case. This is consistent with the fact that in the Aubry model there is an energy-independent metal–insulator transition at $\lambda = 2$, which separates the region $\lambda < 2$ where all states are extended and $\lambda > 2$, where all states are localized.

Figure 2(*a*) shows the transmittance at the band centre $E = 0$ (full curve) and at $E = 0.5$ (broken curve) of a more general Harper model with $\gamma = 0.5$ as a function of λ. At $\lambda = 0$ (Bloch case), $T(E) = 1$ as expected for both the energies. $T(E) \to 0$ as $\lambda \to 2$ for both the energies. For $E = 0.5$, $T(E)$ becomes very small beyond $\lambda = 1.5$ but truly vanishes only for $\lambda > 2$. This shows very clearly that, for the Harper model with $0 < \gamma < 1$, there exist mobility edges with $E_c = \pm(2V - \lambda)$. Since in this plot we have fixed E and plotted only positive λ-values, this shows up as the existence of a metal–

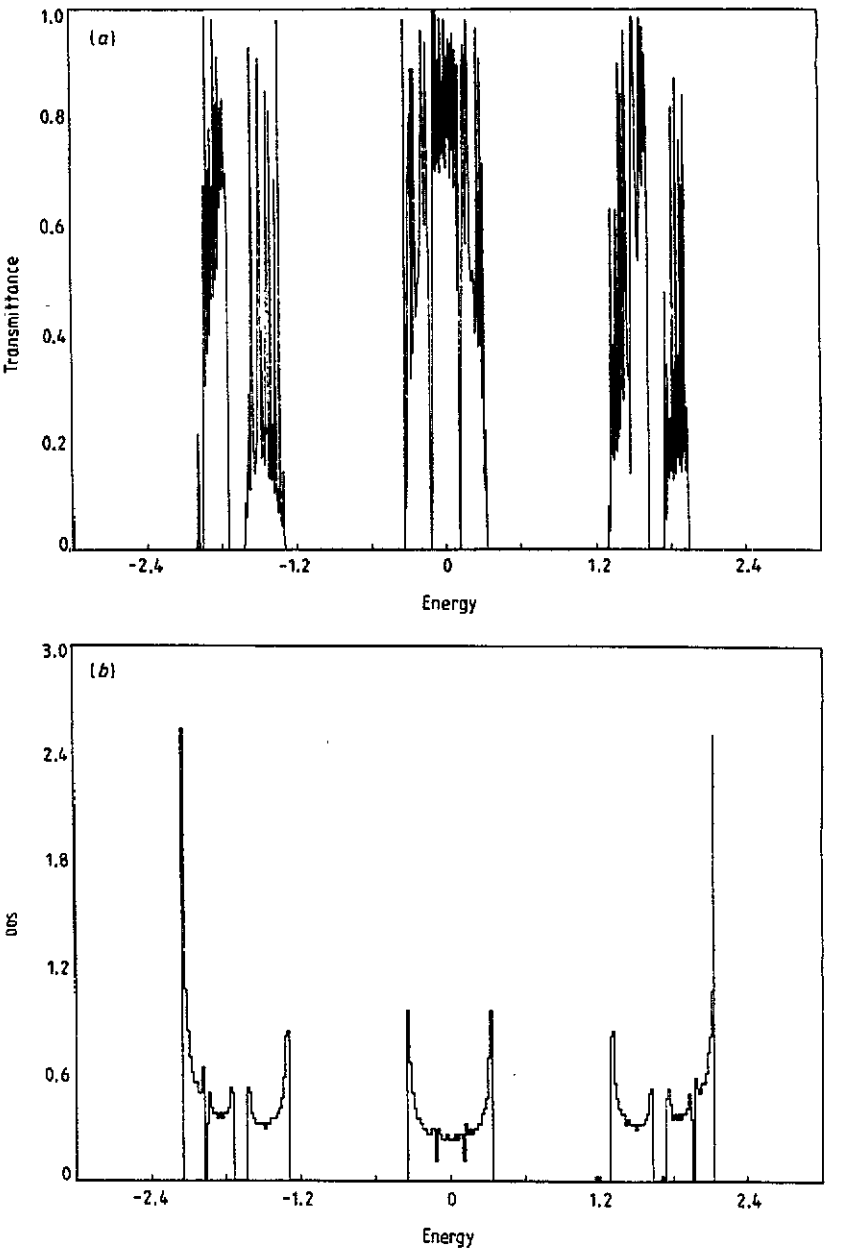

Figure 1. (*a*) Transmittance versus energy of the incoming wave for the Aubry model for $\lambda = 1$. (*b*) The DOS for the Aubry model for $\lambda = 1$.

insulator transition at $\lambda_c = 2V - E$. The existence of very small values of the transmittance for $\lambda > 1.5$ for the $E = 0.5$ case is simply due to finite-size effects. This is shown in figure 2(*b*). Below $\lambda \approx 1.49$ the logarithm of the transmittance is virtually independent of size. Around $\lambda = 1.49$ the transmittance drops exponentially showing exponential localization and with an exponent increasing with increasing size. We should emphasize

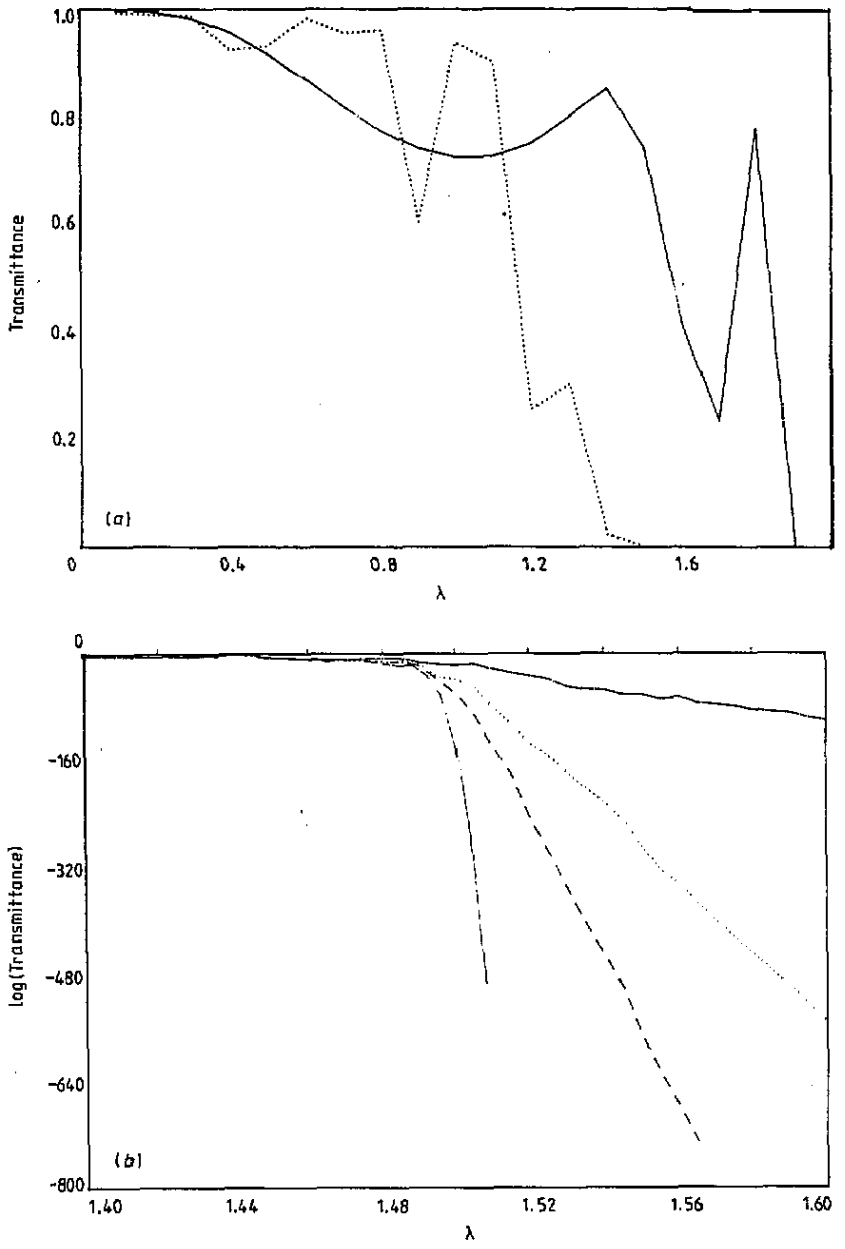

Figure 2. (*a*) Transmittance at $E = 0$ (———) and at $E = 0.5$ (· · · · ·) for the Harper model with $\gamma = 0.5$, as a function of λ. (*b*) Logarithm of transmittance at $E = 0.5$ versus λ at around $\lambda_c = 1.5$ for the above Harper model, showing the effect of finite size on the metal–insulator transition: —·—, 2×10^3; · · · · ·, 10^4; – – –, 4×10^4; ——, 10^5.

here that this method of location of the metal–insulator transition is computationally easy and fast (taking a CPU time of 21.75 s on a HP 9000/300 desktop computer for a single value of λ or E and a system size of 10^5) and does not require cumbersome formulae

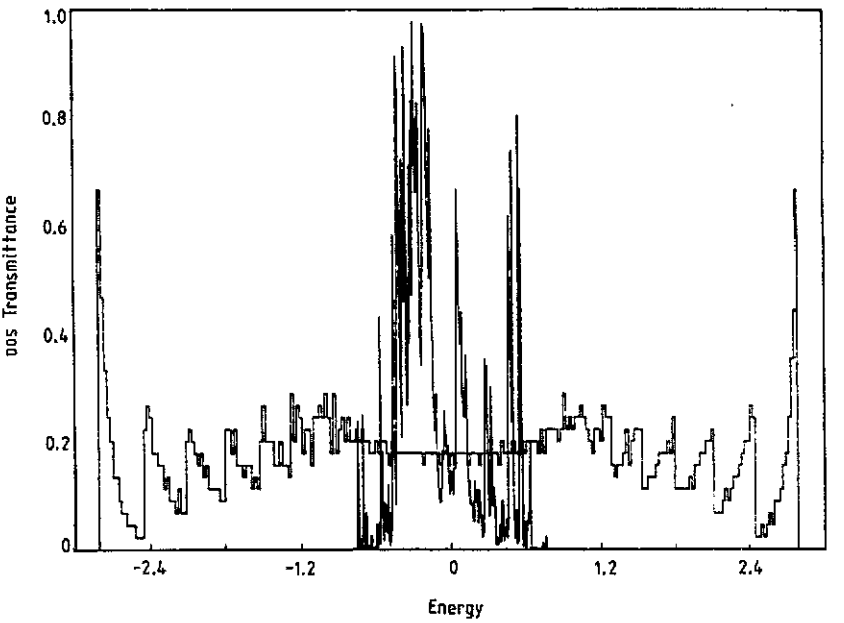

Figure 3. The DOS (scaled up by a factor of 10) and the transmittance versus energy, for the Harper model with $\gamma = 0.7$ and $\lambda = 1$. The mobility edges are clearly seen.

for calculating the localization length involving diagonalization of very large matrices, and assumptions of exponential localization. Indeed, as seen from figure 2(*b*), we need not go to system sizes larger than 10^4 for locating the mobility edges. Moreover, we may use our methodology to analyse situations where we have non-exponential localization.

Figures 3, 4 and 5 show the DOS and the transmittance as a function of energy for the Harper model with $\lambda = 1$ and $\gamma = 0.7, 0.5$ and -2.0, respectively. In the first two cases there exist mobility edges at $E_c = \pm 1$ since $V = \lambda = 1$. The case of negative γ needs special mention and we do that later. In figures 3 and 4 the non-analyticity of the DOS in the localized regime is evident from the rapid fluctuations in that region in contrast with the relatively smooth behaviour in the extended regime. This contrast is more apparent in figure 3 ($\gamma = 0.7$) than in figure 4 ($\gamma = 0.5$) since the localization length tends to infinity as $\gamma \to 0$ (Bloch case). The more elaborate DOS calculations of Das Sarma *et al* on much larger systems are qualitatively similar although they show unsmooth behaviour in the localized regime with an integrable divergence at E_c much more transparently.

Let us discuss the location of band and mobility edges for the Harper model. We can easily understand this from the following discussion put forward by Das Sarma *et al* for positive-γ models. Let us first note that

$$d\varepsilon_n/dn = -[2\lambda\gamma n Q n^{\gamma-1} \sin(2\pi n^\gamma Q)]. \tag{13}$$

For all $\gamma < 1$, this vanishes as $n \to \infty$, since $|\varepsilon_{n+1} - \varepsilon_n| \sim O(n^{\gamma-1})$, i.e. *locally* the ε_n-values do not change much. If one assumes that the wavefunction amplitudes $\varphi_n \sim z^n$, then substituting this in the Schrödinger equation, one obtains

$$z^2 - C_n z + 1 = 0 \tag{14}$$

where $C_n = E - \varepsilon_n$. If $C_n^2 \leqslant 4$, then z is complex, and $|z| = 1$ as appropriate for extended

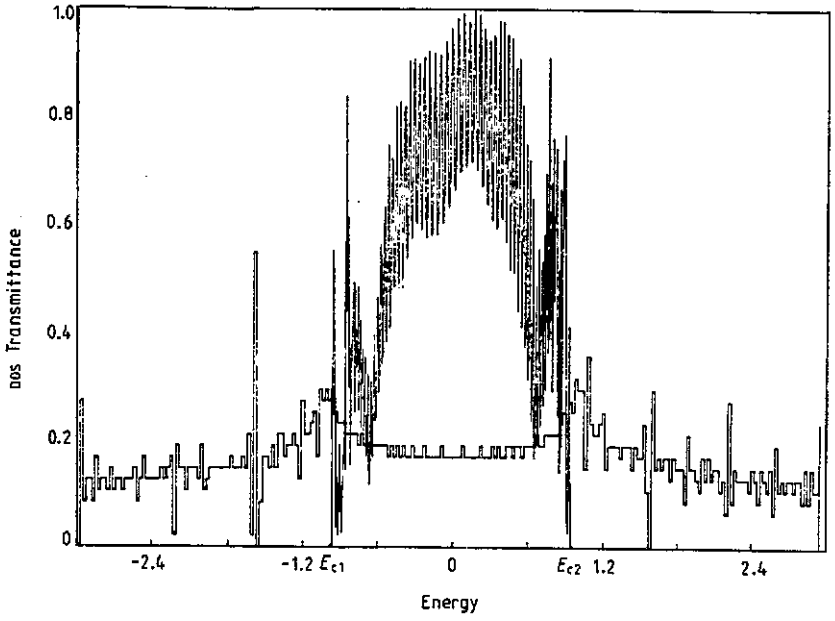

Figure 4. Same as in figure 3 but with $\gamma = 0.5$.

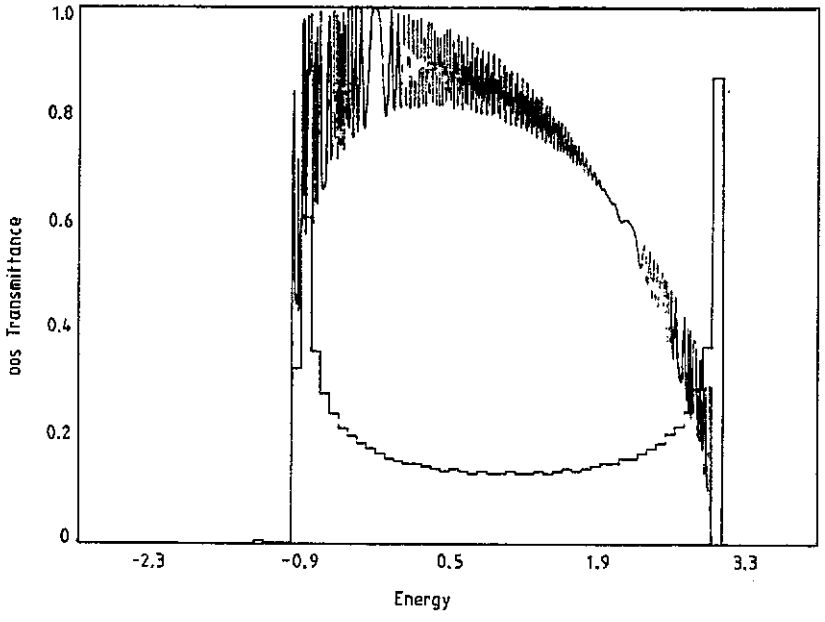

Figure 5. Same as in figure 3 but with $\gamma = -2$.

states. For large n, although ε_n is locally constant, it can take any value between $-\lambda$ and $+\lambda$ for the case $0 < \gamma < 1$. Thus, if the maximum possible positive value of C_n, namely $(C_n)_{\max} \equiv E + \lambda \leqslant 2$, i.e. if $E \leqslant 2 - \lambda$, then the condition of complexity of z is satisfied

for *all* large n. Similarly, if the minimum possible negative value, namely $(C_n)_{\min} \equiv E - \lambda \geq -2$, i.e. if $E \geq -(2 - \lambda)$, again the condition of complexity of z is satisfied for *all* large n. Thus, for $0 < \gamma < 1$, the mobility edges were earlier (Das Sarma *et al* 1990) predicted to be at $\pm(2 - \lambda)$, while band edges are at $\pm(2 + \lambda)$. We see from figures 3 and 4 that, although the effect of the metal–insulator transition clearly shows up in the transmittance as a function of energy, finite-size effects cause the DOS to shrink inside the band edges, particularly as $\gamma \to 1$.

We discuss the case of negative γ somewhat more elaborately since it does not seem to have been mentioned in the literature before. We see in figure 5 for the case $\gamma = -2.0$ that the DOS has its centre shifted to $E = \lambda$ and the mobility edges are at $-2 + \lambda$ and $2 + \lambda$. This asymmetric shift of the centre is common to Harper model with all negative γ (in the large-length limit).

For the case $\gamma < 0$, the argument of the trigonometric functions in equation (13) and in the model potential approaches zero for large n. Thus, for negative values for γ and large n, the site energies ε_n do not alternate in sign and approach a globally constant value of $+\lambda$, the approach being more rapid for larger absolute value of γ. Thus, asymptotically the band edges shift to $-(2 - \lambda)$ and $(2 + \lambda)$, with the band centre being shifted to λ (in comparison with the case of positive γ, where the band centre was at 0). It may be noted that, for small values of n close to the origin, the site energies have not yet reached the constant asymptotic value and hence give rise to some band states in the domain $[-(2 + \lambda), -(2 - \lambda)]$, but the weighting of these states in the DOS become smaller as the chains become larger. This is the reason why we can see a few states in the DOS in figure 5 ($\gamma = -2.0$ and $\lambda = 1$) between $E = 3.0$ and $E = -1.0$. As for the condition for complexity of the solutions for z, we now have $(E - \lambda)^2 \leq 4$. Thus, the mobility edges are at $-(2 - \lambda)$ and $2 + \lambda$. Thus asymptotically almost *all* states are extended for $\gamma < 0$, even though for finite-size chains this statement is not exact. It is thus interesting to note here that, for $\gamma = 0$, all states are extended (Bloch states), but such is not the case for $\gamma \neq 0$. Thus, $\gamma = 0$ seems to be a singular point.

One of the statements often made is that localization results from the randomization of the phase of the wavefunction as it travels through the system. To study this phenomenon for the present model, in figure 6 we have plotted the Argand map of the complex transmission coefficient, i.e. its imaginary versus real part, as the size of the system varies. This is directly related to the Argand map of the outgoing wavefunction.

At $\lambda = 1$ for $\gamma = 1$, we have a reasonably well transmitting state (figure 6). The Argand map is a regular curve with a few Fourier components. As λ increases, the maps pick up more Fourier components and resemble more complicated Lissajous figures. The scatter about the base curve also increases. The average absolute amplitude remains reasonably close to unity, as is seen from figure 6 with λ up to 1.8. At around $\lambda = 2.0$, the transmittance precipitately goes down to zero, and the Argand maps collapse to a point for $\lambda \geq 2.0$ for large enough lengths.

In figure 6(*c*) we have shown enlargements of the Argand maps for the cases $\lambda = 1.98$, 2.0 and 2.02. These are on either side of the critical state $\lambda_c = 2$. For $\lambda = 1.98$ the map clearly has not collapsed at least to the sizes that we have worked with. However, it has a wide spread. For $\lambda = 2.02$, the map clearly spirals in towards zero. The critical state $\lambda_c = 2$ shows a widely random spread and no collapse, at least up to the sizes that we have worked with. However, it must be stated that it has been noted in studies of conductance (Thakur *et al* 1990) that for λ very near but greater than the critical λ_c the logarithm of conductance goes to zero in steps which become quite long as λ approaches λ_c. Thus the map for a *just* localized state may appear not to collapse for very large sizes

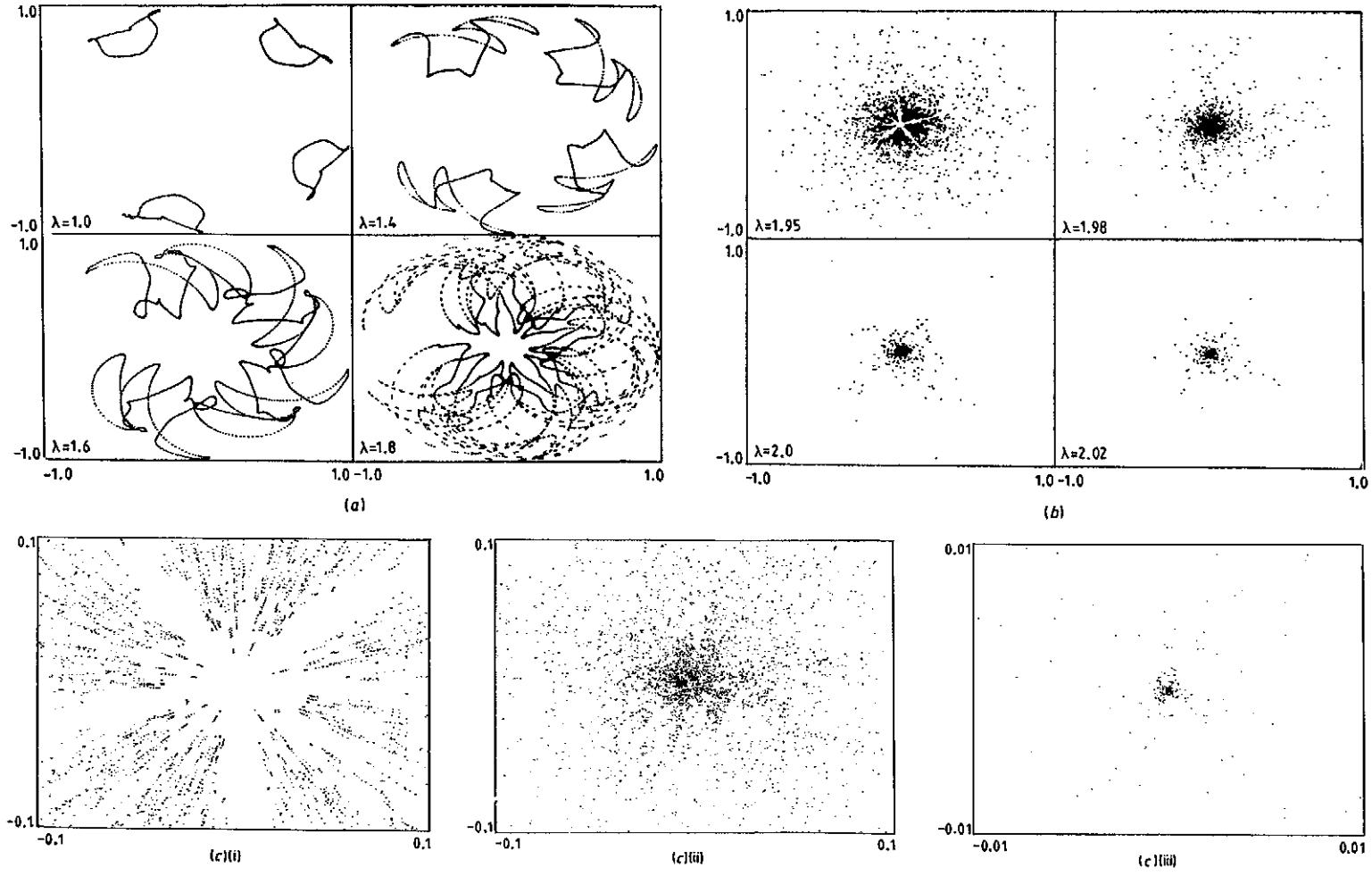

Figure 6. (*a*) Argand maps of the complex transmission coefficients for the Aubry model at $E = 0$ and $\lambda = 1.0$, 1.4, 1.6 and 1.8. (*b*) Same as in (*a*) with $\lambda = 1.95$, 1.98, 2.0 and 2.02 where $\lambda_c = 2.0$. (*c*) Enlarged maps of (*b*) with (i) $\lambda = 1.98$, (ii) $\lambda = 2.0$ and (iii) $\lambda = 2.02$.

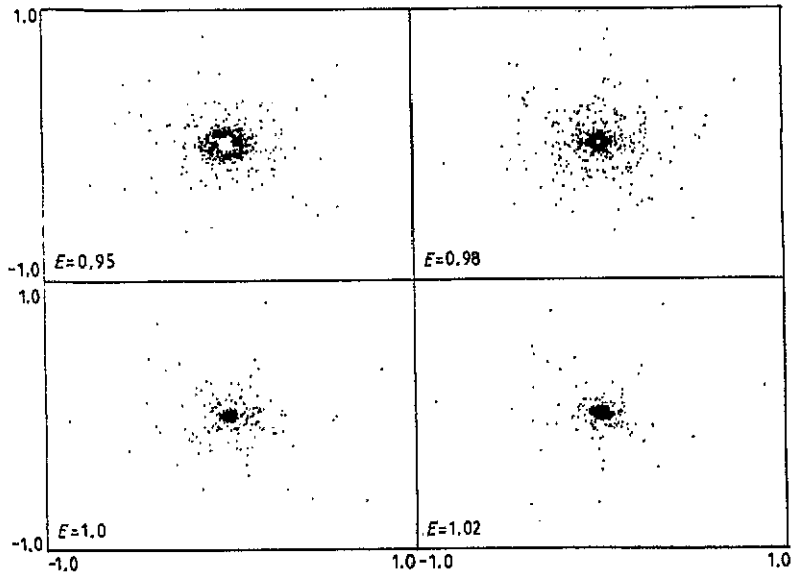

Figure 7. Argand maps for the Harper model with $\gamma = 0.5$ and $\lambda = 1$ at $E = 0.95, 0.98, 1.0$ and 1.02 where $E_c = 1.0$.

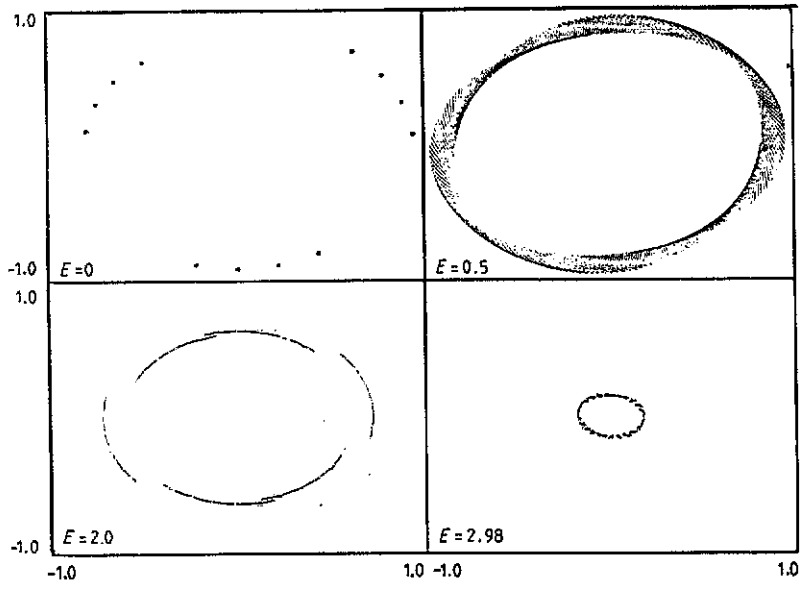

Figure 8. Argand maps for $\lambda = 1.0$, $\gamma = -2.0$ for $E = 0, 0.5, 2.0$ and 2.98.

and eventually shows collapse only when we reach sizes of the order of 10^7–10^8. This extent of uncertainty in the location of the critical values is inherent in any numerical work.

In figure 7 we show Argand maps for fixed $\gamma = 0.5$ and $\lambda = 1$ at different energies near the mobility edge at $E_c = 1.0$. The behaviours of the maps are very similar to the

λ-driven transition shown in figure 6. On the extended side the maps are scattered around closed Lissajous figures. This scatter increases as we approach the mobility edge, becoming almost random very near it. Beyond the mobility edge the maps collapse into the origin.

In figure 8 we show the Argand maps for $\gamma = -2.0$ and $\lambda = 1$ for four different energies within the band: $E = 0, 0.5, 2.0$ and 2.98. All the maps are regular maps without random scatter or collapse except exactly at the band edges (which are also the mobility edges for negative γ). Except at special energies such as $E = 0$ and 2.0 (shown here), the maps are distorted circles. The distortion is due to the quasi-periodicity in the problem. At the special energies $E = 0$ and 2.0, as we increase the size, no new sectors appear. The only effect is the filling up of the existing sectors in the map.

It would be interesting to Fourier analyse the maps and to study their spectrum. We expect the spectrum to change from a finite set of frequencies in the extended regime to a continuum in the localized regime, characteristic of chaotic maps. We shall report this in a subsequent publication.

Acknowledgments

One of the authors (AM) would like to thank Professor Abdus Salam, IAEA and UNESCO, for hospitality at the ICTP, Trieste, where a part of this work was carried out. He would also like to thank SAREC for financial support during his visit to ICTP under the Associateship scheme. AM would like to thank DST, India, under whose Project he carried out this work. CB would like to thank the CSIR for financial assistance during her research work. AKS would like to thank Dr B K Chakrabarti and Dr S Bhattacharjee for several useful discussions.

References

Anderson P W 1958 *Phys. Rev.* **109** 1492
Andre G and Aubry S 1980 *Ann. Israel Phys. Soc.* **3** 133
Avron J and Simon B 1982 *Bull. Am. Math. Soc.* **6** 81
Das Sarma S, Song He and Xie X C 1990 *Phys. Rev.* B **41** 5544
Godin T J and Haydock R 1988 *Phys. Rev.* B **38** 5237
Griniasty M and Fishman S 1988 *Phys. Rev. Lett.* **60** 1334
Ishii K 1973 *Prog. Theor. Phys. Suppl.* **53** 77
Kohmoto M and Banavar J R 1986 *Phys. Rev.* B **34** 563
Kohmoto M, Kadanoff L P and Tang C J 1983 *Phys. Rev. Lett.* **50** 1870
Kumar N and Thakur P K 1990 *Preprint* 556 International Centre for Theoretical Physics, Trieste
Liu Y and Chao K A 1986 *Phys. Rev.* B **34** 5247
Merlin R, Bajema K, Clarke R, Juang F-T and Bhattacharya P K 1985 *Phys. Rev. Lett.* **55** 1768
Simon B 1982 *Adv. Appl. Math.* **3** 463
Sokoloff J B 1983 *J. Phys. C: Solid State Phys.* **17** 1703
—— 1985 *Phys. Rep.* **126** 189
Souillard B 1987 *Chance and Matter (Les Houches)* ed J Souletie, J Vannimenus and R Stora (Amsterdam: Elsevier) session XLVI
Tang C and Kohmoto M 1986 *Phys. Rev.* B **34** 2041
Thakur P K, Brouers J and Ananthakrishna G 1990 *Preprint* 555 International Center for Theoretical Physics, Trieste
Thouless D J 1988 *Phys. Rev. Lett.* **61** 2141